# Surface electronic structure and magnetic properties of doped manganites

M. J. Calderón

*Instituto de Ciencia de Materiales (CSIC), Cantoblanco, 28049 Madrid, Spain*
*and Departamento de Física Teórica de la Materia Condensada, Universidad Autónoma de Madrid, 28049 Madrid, Spain*

L. Brey and F. Guinea

*Instituto de Ciencia de Materiales (CSIC), Cantoblanco, 28049 Madrid, Spain*
(Received 22 March 1999)

The electronic structure and magnetic properties of doped manganites surfaces are investigated. It is assumed that, at the outermost layer, the environment of the Mn ions does not have cubic symmetry. The $e_g$ orbitals are split and the double exchange mechanism is weakened. The charge state of the Mn ions is modified, and the magnetic ordering of the spins tends to be antiferromagnetic. The surface magnetization and the dependence of the transport properties through the resulting surface barrier on applied magnetic field and temperature is analyzed. [S0163-1829(99)02430-3]

## I. INTRODUCTION

Doped manganites show many unusual features, the most striking being the colossal magnetoresistance in the fully ferromagnetic phase.[1,2] Extensive research shows that the transport properties, and the magnetoresistance in particular, are significantly modified at artificially created barriers[3–10] or in ceramic materials.[11–15] The magnetoresistance has larger values at low fields, and persists at large fields, unlike in the bulk case. The relevance of the interfaces in perovskite manganites can also be inferred by comparing with transport in related materials which exhibit colossal magnetoresistance.[16] These properties have been ascribed to changes in the interface structure, although the origin of these modifications and the resulting structure are not known.

In the present paper, we analyze the simplest, and most common, modification with respect to the bulk that a surface may show: the loss of cubic symmetry around the Mn ions. It is well known that $La_{1-x}A_xMnO_3$ shows a transition from a tetragonal (or orthorhombic) structure to a cubic one as the value of the doping $x$ is increased. The systems with the highest Curie temperature correspond to $x \sim \frac{1}{3}$ and are in the cubic phase. This implies that the two $e_g$ orbitals of the Mn ion are degenerate and contribute to the conduction band. In this situation, the double exchange mechanism is enhanced.

The cubic symmetry is lost at the surface. If the last layer is oxygen deficient, the resulting splitting between the $e_g$ orbitals can be larger than typical Jahn-Teller splittings in $La_{1-x}A_xMnO_3$ with small values of $x$. When one of the $e_g$ orbitals moves away from the Fermi level, the double exchange mechanism is weakened, and direct antiferromagnetic couplings between the core $S = \frac{3}{2}$ spins can prevail. Moreover, the reduction in electronic kinetic energy can also lead to charge transfer between the surface layers and the bulk, contributing to the formation of a surface dipole. All these effects can be modified by surface spin waves, which, in turn, depend on temperature and external magnetic fields. A significant dependence of the metal-insulator transition temperature as function of oxygen pressure in thin films is found in Ref. 17.

## II. THE MODEL

In order to investigate these features, we start from a tight binding Hamiltonian, using the two $e_g$ orbitals, $d_{x^2-y^2}$ and $d_{3z^2-r^2}$, which we designate $x$ and $z$, respectively. Hopping between them takes place through virtual jumps to the intermediate O ions. Fixing the orientations of the $e_g$ orbitals to the frame of reference of the lattice, we obtain for the $z$ direction,

$$t_{zz} = t,$$
$$t_{xz} = t_{xx} = 0 \tag{1}$$

and for the directions in the $x$-$y$ plane,

$$t_{zz} = \frac{1}{4}t,$$
$$t_{xz} = \pm \frac{\sqrt{3}}{4}t,$$
$$t_{xx} = \frac{3}{4}t, \tag{2}$$

where the two signs in $t_{xz}$ correspond to the $x$ and $y$ directions, and $t$ is the effective $e_g - e_g$ hopping generated from the $(dp\sigma)$ matrix element between a $d$ orbital in a given Mn ion, and a $p$ orbital in a neighboring O ion.[18,19] At each site there is also a spin, from the three $t_{2g}$ orbitals, which we treat as classical, and parametrize in terms of the polar angles $\theta$ and $\phi$. We assume that the Hund's coupling between the $e_g$ electrons and this spin is much larger than other scales in the model. Then, the hopping elements depend on the orientation of the core spins, and the actual hopping is[20]

$$t_{\alpha,\beta}^{i,j} = t_{\alpha,\beta} \left( \cos\frac{\theta_i}{2}\cos\frac{\theta_j}{2} + \sin\frac{\theta_i}{2}\sin\frac{\theta_j}{2} e^{i(\phi_i - \phi_j)} \right), \tag{3}$$

where the value of the hopping has been estimated to be $t \sim 0.1-0.3$ eV.

PRB <u>60</u>    6698

We study a cubic lattice with periodic boundary conditions in the $x$ and $y$ directions, and open boundary conditions along the $z$ direction, where two (001) surfaces terminate the lattice. We use slabs with a thickness of 20 atoms. We have checked that, for this size, the bulk properties are recovered at the center of the slab. The environment of the outermost Mn ions is deficient in oxygen. The oxygen octahedra which surround the Mn ions are incomplete. The absence of the negatively charged $O^{2-}$ ions leads to a downward shift of the $e_g$ levels with respect to the values in the bulk. This shift is larger for the $d_{3z^2-r^2}$ orbital, which points towards the surface. The $d_{x^2-y^2}$ orbital is more localized around the ion, and is less sensitive to the change in the environment. In order to keep the number of free parameters in the model to a minimum, we leave the $d_{x^2-y^2}$ level unchanged with respect to the bulk, while the $d_{3z^2-r^2}$ is shifted downwards by an amount $\Delta$. The value of $\Delta$ should be comparable, or larger, than the observed Jahn-Teller splitting in LaMnO$_3$, which, in turn, is larger than the $e_g$ bandwidth. Reasonable values of $\Delta$ are $\sim 0.5-1.5$ eV.[2] The $e_g$ levels at all other layers remain unchanged, except for electrostatic effects.

This shift of the surface $d_{3z^2-r^2}$ orbitals leads to charge transfer between the bulk and the surface. We treat the induced electrostatic effects within the Hartree approximation. This gives rise to an additional shift in the electronic levels which is determined by solving self-consistently the Schrödinger and Poisson equations. This electrostatic shift is equal for the two $e_g$ orbitals at each layer. Screening from other levels is described in terms of a dielectric constant of value $\epsilon = 5\epsilon_0$.[21] Self-consistency is imposed on the $e_g$ levels in all layers in the system. We do not consider the possibility of orbital order induced by a Hubbard $U$ between electrons at the two $e_g$ orbitals.[22] We analyze underdoped materials, $x < 0.5$, where no unusual magnetic ordering is expected.[23] The Hartree approximation acts to suppress charge fluctuations, although it does not split the $e_g$ bands in the way a Hubbard term does. This effect should be less important at the surface, due to the crystal field splitting $\Delta$ introduced before.

## III. RESULTS

### A. Surface electronic structure

Typical results, for $\Delta = 10t$, hole concentration of $x = 0.3$ and a ferromagnetic configuration of all spins are shown in Fig. 1. Charge neutrality corresponds to a total occupancy of the $e_g$ orbitals of 0.7.

The large splitting between the $e_g$ orbitals at the surface leads to a significant charge transfer to the outermost layer. The charge distribution reaches the bulk values at the third layer, in agreement with the expected short screening length of the metal. The surface $d_{3z^2-r^2}$ orbitals are almost full, while the $d_{x^2-y^2}$ are empty, so that the charge state of the ion is Mn$^{3+}$. Hence, for the value of $\Delta$ used in Fig. 1, the double exchange mechanism is almost completely suppressed at the surface. Then, it is likely that antiferromagnetic interactions will prevail at the surface. Electronic properties due to ferromagnetic and antiferromagnetic ordering at the surface are compared in Fig. 2, where we show the total charge and the charge in the $d_{3z^2-r^2}$ orbital for the outermost level as a function of $\Delta$.
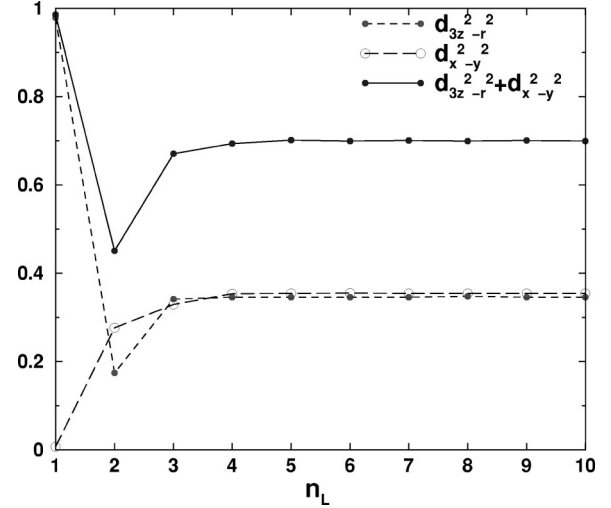


FIG. 1. Charge in the $e_g$ orbitals as a function of the distance from the surface for the ferromagnetic configuration and $\Delta = 10t$. On the surface, $n_L = 1$, the $x$ orbitals are almost empty, due to the shift $\Delta$.

Higher values of $\Delta/t$ do not alter these results. For intermediate values of $\Delta/t$, the surface electrostatic barrier depends significantly on the magnetic configuration. The surface $d_{x^2-y^2}$ orbitals are practically empty, and the $d_{3z^2-r^2}$ are occupied for $\Delta > 3t$.

### B. Surface magnetic order

The suppression of the double exchange ferromagnetic coupling at the surface leads to an enhancement of the superexchange interaction among the Mn ions. To investigate further this effect, we study magnetic configurations where the core spins of the surface Mn ions are allowed to rotate, as shown in Fig. 3. The canting angle $\theta$ is used as a variational parameter which allows us to change continuously from ferromagnetic to antiferromagnetic surface ordering. $\theta = 0$ means perfect ferromagnetic order at the surface. $\theta = \pi/2$ gives rise to an antiferromagnetic alignment of the surface spins, at right angles with the bulk magnetization. To take into account the superexchange interaction, we introduce an antiferromagnetic coupling between the Mn core spins. Subtracting a trivial constant, the energy per surface ion, due to this coupling, is

$$E_{AF} = J_\perp \cos\theta + 2J_\parallel \cos 2\theta, \qquad (4)$$

where $\theta$ is the angle shown in Fig. 3, $J_\perp$ is the antiferromagnetic coupling between a Mn spin at the surface and one in the next layer, and $J_\parallel$ is the coupling between spins at the surface layer. From symmetry considerations, $J_\parallel = 4J_\perp$.[24]

We now estimate, for a given value of $\Delta$, the surface antiferromagnetic coupling needed to stabilize antiferromagnetic or canted structures at the surface. We calculate the total energy of the system for the magnetic ordering depicted in Fig. 3.

The total energy of the system is the sum of the electronic energy $E_0$ (kinetic plus Hartree) and antiferromagnetic energy. The $E_0$ contribution, and the antiferromagnetic exchange energy are shown in Fig. 4. The exchange coupling chosen is comparable to that between two Mn$^{3+}$ ions in un-
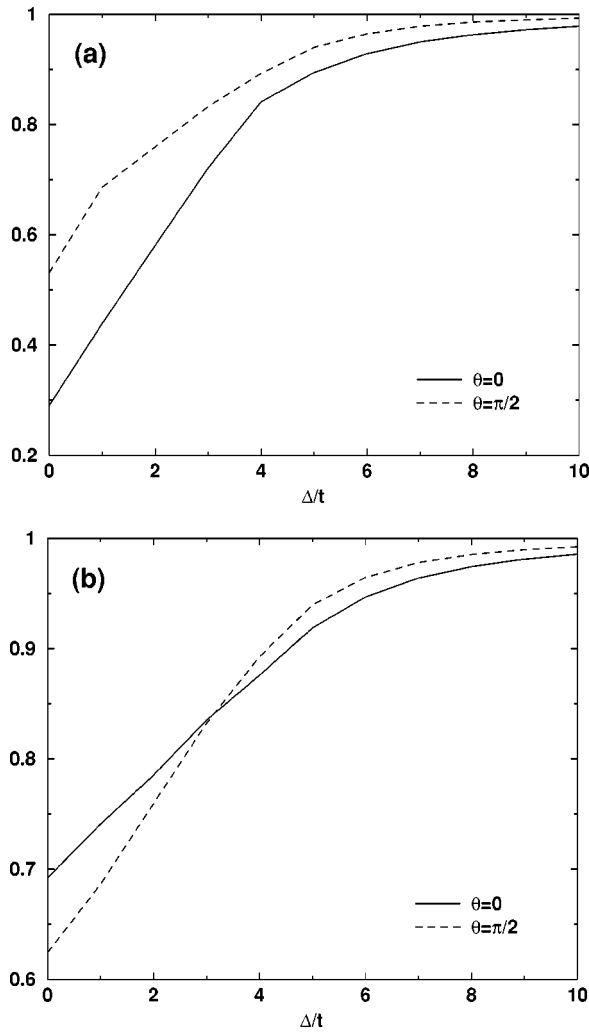
FIG. 2. Charge in the $d_{3z^2-r^2}$ orbital (a) and total charge (b) versus $\Delta/t$. $\theta=0$ corresponds to a ferromagnetic ordering. $\theta=\pi/2$ corresponds to the antiferromagnetic surface ordering described in the text (see also Fig. 3).

doped LaMnO$_3$. This is probably an underestimate of the exchange at the surface.[24,25] The electronic energy has a minimum at $\theta=0$ because the absolute value of the kinetic energy is maximum. On the other hand, at $\theta=\pi/2$, the surface kinetic energy is minimum, corresponding to a maximum in $E_0$. The difference in energy between these extreme
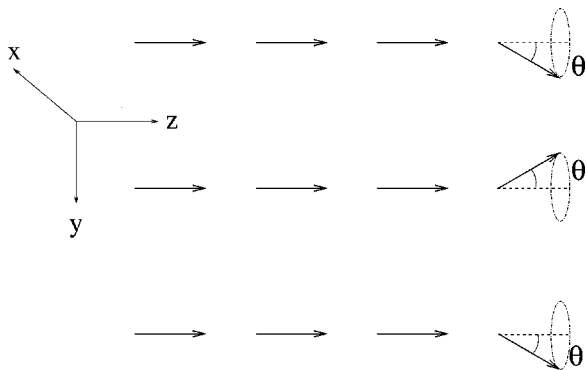


FIG. 3. Magnetic structure considered in the text. Only the spins at the surface layer are rotated, in the way shown.
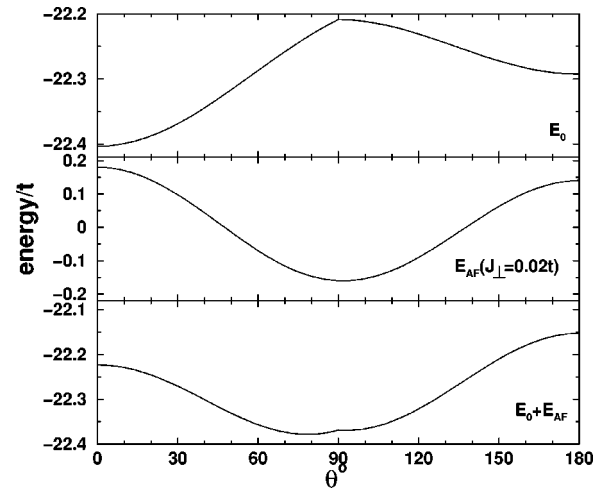


FIG. 4. Electronic energy (top), magnetic energy (middle) and sum of the two (bottom) as function of the canting angle $\theta$ shown in Fig. 3. $\Delta/t=10$. $J_\perp=0.02t$ in Eq. (4).

values of $E_0$ decreases as $\Delta$ increases. On the contrary, $E_{AF}$ has a minimum at $\theta=\pi/2$ corresponding to antiferromagnetic ordering on the surface. By minimizing the total energy $E_0+E_{AF}$ as a function of $\theta$ we obtain the canting angle as a function of the antiferromagnetic coupling $J_\perp$.

Figure 5 shows the calculated phase diagram as function of the splitting at the surface between the $e_g$ levels, $\Delta$, and the direct antiferromagnetic coupling between the core spins $J_\perp$, for two different values of the hole concentration. The effect of $J_\perp$ is increased as $\Delta$ becomes larger, destroying the ferromagnetic order on the surface. In fact, for realistic values of the couplings, the surface spins are aligned almost antiferromagnetically with respect to those of the bulk. Note that the constraints imposed on the spin orientations will underestimate this tendency towards antiferromagnetism, as we do not allow to relax the spins in the layers deeper into the surface.

The changes in the magnetic surface structure also lead to modifications in the spin stiffness at the surface, which is
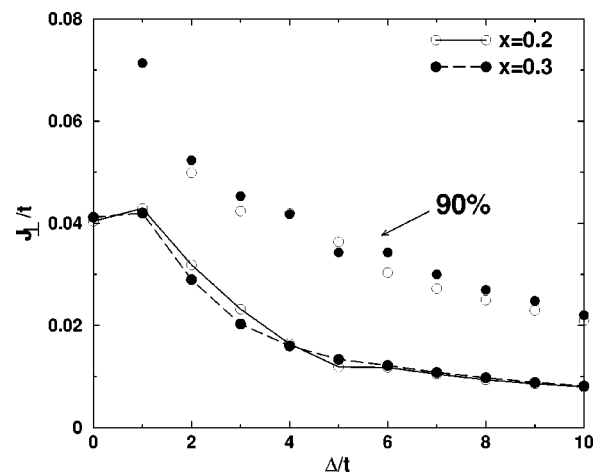


FIG. 5. Magnetic phase diagram of the surface of a doped manganite. The lines separate the fully ferromagnetic and the canted regions. The dots indicate that the order is 90% antiferromagnetic, namely, $\theta=81°$. Full dots are results for hole concentration of $x=0.3$. Open dots are for $x=0.2$.
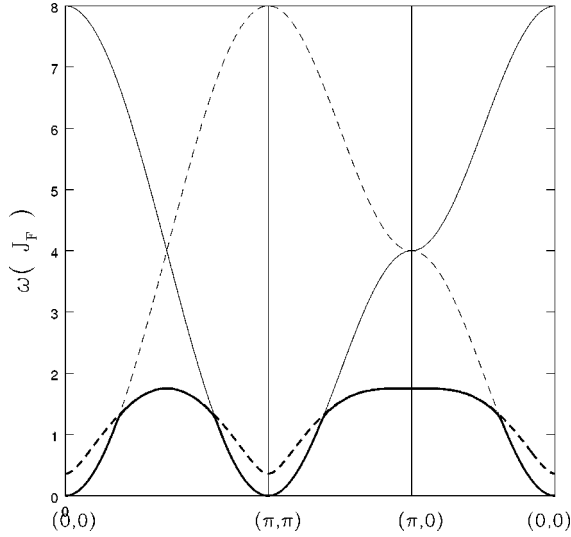
FIG. 6. Projected magnetic structure at an antiferromagnetic surface weakly coupled to the ferromagnetic bulk (see text). The surface antiferromagnetic coupling is $J_{AF}=0.5J_F$ and the ferromagnetic coupling to the next layer is $J_F'=0.3J_F$, where $J_F$ is the ferromagnetic coupling in the bulk. Energies are shown in units of $J_F$. The bands are shown in the projected ferromagnetic Brillouin zone. The thin lines denote the lowest edge of the bulk continuum. Note the folding induced by the antiferromagnetic structure.

weaker than in the ferromagnetic bulk. It is straightforward to show that weaker couplings lead to the formation of bands of surface magnons.[26] We analyze the surface bands by means of the Schwinger boson approximation, which gives a realistic spectrum for the bulk bands of double exchange systems.[27] We assume that there is a direct antiferromagnetic coupling $J_{AF}$ between the spins at the outermost layer, a weak ferromagnetic coupling between these spins and those at the nearest layer, $J_F'$, and that the bulk values for the ferromagnetic couplings are recovered at the second layer and beyond, $J_F$. Assuming perfect translational invariance in the directions parallel to the surface, the magnetic structure at the last layer is described by the Green's function:

$$\mathcal{G}_{0,0}(\vec{k}_\parallel,\omega)=\begin{bmatrix} \langle b_{\vec{k}_\parallel\uparrow}^\dagger(\omega)b_{\vec{k}_\parallel\uparrow}\rangle & \langle b_{\vec{k}_\parallel\uparrow}^\dagger(\omega)b_{\vec{k}_\parallel+\vec{Q}_\parallel\downarrow}^\dagger\rangle \\ \langle b_{\vec{k}_\parallel\uparrow}^\dagger(\omega)b_{\vec{k}_\parallel+\vec{Q}_\parallel\downarrow}\rangle & \langle b_{\vec{k}_\parallel+\vec{Q}_\parallel\downarrow}^\dagger(\omega)b_{\vec{k}_\parallel+\vec{Q}_\parallel\downarrow}\rangle \end{bmatrix}.$$
$$(5)$$

The operators $b_{\vec{k}_\parallel s}$ destroy excitations of momentum $\vec{k}_\parallel$ and spin $s$ at the outermost layer. The vector $\vec{Q}=(\pi,\pi)$ describes the antiferromagnetic superstructure. A recursive equation can be written for Green's functions of the type $\mathcal{G}_{n,0}$, leading to a full solution of the problem. Details are given in the Appendix.

The magnetic modes at a (1,0,0) surface are given in Fig. 6. We find the bulk continuum and two types of surface states: a band located very close to the edge of the continuum, with slow decay into the bulk, and a band which tends to reproduce the linear dispersion of an isolated single layer, except for a gap at (0,0). This gap is proportional to $J_F'$ when $J_F'\ll J_{AF},J_F$. This band overlaps with the bulk continuum, but cannot decay into it because of its symmetry. The spectrum, at very low energies, is determined by the
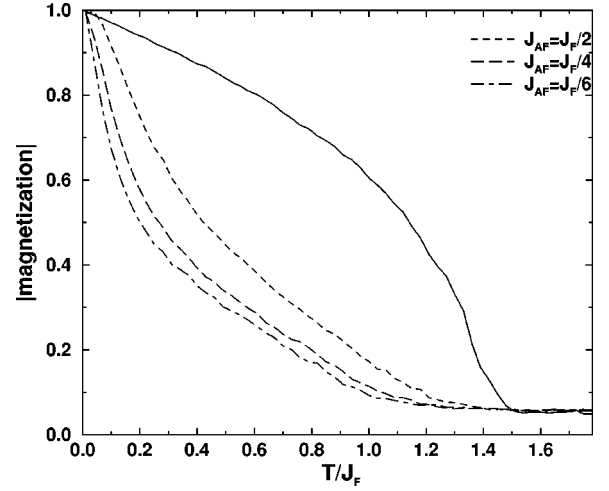


FIG. 7. Magnetization of the last layer as a function of temperature for a cluster with 20 layers and open boundary conditions. For comparison, the results for a cluster of the same size and periodic boundary conditions (no surfaces) are also shown.

bulk modes, and the states derived from them. At higher energies, the surface excitations at energies $\sim J_{AF}$ have the largest spectral weight. Thermal excitation of these modes leads to a decay of the surface magnetization as function of temperature which is faster than in the bulk. In order to estimate this effects, we have calculated, using Monte Carlo techniques,[28] the surface magnetization of a cluster of classical spins. In this model, the bulk double exchange mechanism is described by an effective ferromagnetic Heisenberg coupling $J_F$, and the surface spins interact with an antiferromagnetic coupling $J_{AF}$. The outermost spins interact with the spins in the second layers via a ferromagnetic coupling $J_F'$. From the results reported previously, we estimate that $J_F'$ is very small, $\sim -J/100$ and $J_{AF}$ takes a value between $J_F/2$ and $J_F/6$. In Fig. 7 we plot the surface magnetization as a function of the temperature for different values of $J_{AF}$. The results obtained do not depend strongly on the value of $J_{AF}$ and they are in reasonable agreement with the experimental results reported in Ref. 29.

### C. Surface conductance

The combination of energy shifts and changes in the magnetic couplings reduces the conductance of the surface, even in the absence of other, extrinsic, barriers. In order to estimate this effect, we have calculated the resistance between two perfect double exchange ferromagnetic metals separated by a layer with the amount of charge and the magnetic structure obtained in the previous calculations. Since only the $d_{3z^2-r^2}$ orbitals contribute to the transport through the interface, we have simplified the model, and only a single orbital per site is kept. The calculations were done using the method described in Refs. 30 and 31. Two effects contribute to the resistivity, the shift in energy of the interface orbital and the difference in spin orientation between the atoms at the bulk and at the interface. The conductance is sharply reduced when the surface layer is antiferromagnetic, as the double exchange mechanism is suppressed. We find that for hole concentrations of $x=0.3$ the presence of the interface increases the resistance of the system in a factor bigger than
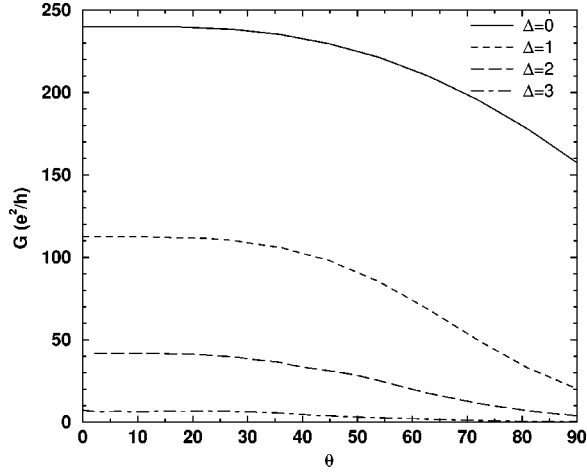
FIG. 8. Conductance through a surface layer of a $20 \times 20$ lattice, as a function of the angle $\theta$, for different shifts of the surface level.

10. The results, as function of this shift and the magnetic order in the layer, are shown in Fig. 8.

A magnetic field will reduce the antiferromagnetism at the surface, and, at high fields, the surface spins are aligned parallel to the bulk. We estimate this effect by adding a magnetic field to the model and finding the magnetic structure which minimizes the energy. The resulting conductance, for $\Delta = 3t$ and $J_\perp = 0.025t$, is plotted in Fig. 9. A very high field $\sim 60$T is required to saturate the magnetoresistance. Note that the low field ($<1$ T) magnetoresistance is probably due to the alignment of the polarization of the bulk electrodes, which can be understood within conventional models.[32,33] Our results for the high field dependence are consistent with the available experimental data.[3–10]

The magnetic excitations of the surface layer also modify the magnetoresistance at finite temperatures.[34–36] Spin flip scattering due to thermally excited magnons leads to a suppression of the magnetoresistance at temperatures below the bulk Curie temperature. The dependence of the magnetoresistance on temperature should be similar to that of the surface magnetization, shown in Fig. 7.

## IV. CONCLUSIONS

We have shown that the lack of cubic symmetry at surfaces, combined with the double exchange mechanism, leads to significant changes in the magnetic and transport properties of doped manganites. Charge is transferred from the bulk to the surface layers, leading to the formation of $Mn^{3+}$ ions at the surface, and to an electrostatic barrier for the electron transport.

The absence of the electronic carriers at the surface implies the weakening of the double exchange mechanism, and the dominance of direct antiferromagnetic interactions between the Mn spins. An antiferromagnetic layer can be formed, for realistic values of the interactions. We have analyzed the surface spin waves, and temperature dependence of the magnetization at the surface. The magnetic disorder at the surface can be considerably larger than in the bulk, leading to spin dependent scattering which reduces the magnetoresistance. Large magnetic fields are required to align the surface moments.
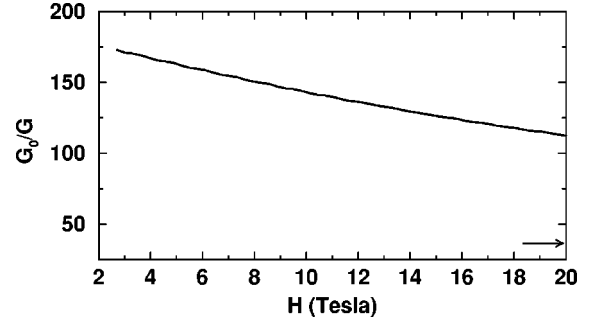


FIG. 9. Inverse conductance, normalized to the conductance of a perfect ferromagnetic system ($\theta = 0$ and $\Delta = 0$), of a magnetic layer, as function of applied field. The arrow indicates the saturation limit at high fields. The size of the system is $20 \times 20 \times 20$. The parameters used are described in the text.

Finally, we have computed the transport properties across the surface. An applied magnetic field enhances the conductance of the barrier, by favoring the double exchange mechanism and the valence fluctuation of the Mn ions. Our results are consistent with a number of experiments on magnetic barriers and granular materials.

## APPENDIX

We outline the calculation of the surface Green's function in the presence of antiferro- and ferromagnetic interactions. As discussed in Sec. III B, we assume that there is a direct antiferromagnetic exchange, $J_{AF}$ between spins at the surface. These spins have a ferromagnetic coupling, $J'_F$, with those at the next layer. The remaining layers have the ferromagnetic coupling appropriate for the bulk, $J_F$.

Cutting off the last layer, $n = 0$, we can write for the remaining layers the equations

$$\omega^2 \mathcal{G}_{1,1}(\vec{k}_\parallel, \omega) = J_F[\mathcal{G}_{2,1}(\vec{k}_\parallel, \omega) - \mathcal{G}_{1,1}(\vec{k}_\parallel, \omega)] \quad (A1)$$

if $n = 1$, and

$$\omega^2 \mathcal{G}_{n,1}(\vec{k}_\parallel, \omega) = J_F[\mathcal{G}_{n-1,1}(\vec{k}_\parallel, \omega) + \mathcal{G}_{n+1,1}(\vec{k}_\parallel, \omega)$$
$$- 2\mathcal{G}_{n,0}(\vec{k}_\parallel, \omega)] \quad (A2)$$

if $n > 1$. These equations can be solved by standard methods, and we obtain

$$\mathcal{G}_{1,1}(\vec{k}_{\parallel},\omega)=\frac{1}{\dfrac{\omega-J_F\epsilon_{\vec{k}_{\parallel}}}{2}-\sqrt{\dfrac{(\omega-J_F\epsilon_{\vec{k}_{\parallel}})^2}{4}+J_F(\omega-J_F\epsilon_{\vec{k}_{\parallel}})}}, \qquad (A3)$$

where $\epsilon_{\vec{k}_{\parallel}}=4+2\cos(k_x)+2\cos(k_y)$.

Once we know the Green's function for the first bulk layer, we can include its coupling to the surface layer by defining an effective self-energy. We find

$$\mathcal{G}_{0,0}^{-1}(\vec{k}_{\parallel},\omega)=\begin{bmatrix} \omega-\lambda-J_F'\cos(\theta/2)-\dfrac{J_F'^2\cos^2(\theta/2)}{\mathcal{G}_{1,1}^{-1}(\vec{k}_{\parallel},\omega)-J_F'\cos(\theta/2)} & J_{\mathrm{AF}}\sin(\theta)\,\gamma_{\vec{k}_{\parallel}} \\[12pt] -J_{\mathrm{AF}}\sin(\theta)\,\gamma_{\vec{k}_{\parallel}} & \omega+\lambda+J_F'\cos(\theta/2)+\dfrac{J_F'^2\cos^2(\theta/2)}{\mathcal{G}_{1,1}^{-1}(\vec{k}_{\parallel}+\vec{Q}_{\parallel},-\omega)-J_F'\cos(\theta/2)} \end{bmatrix},$$
$$(A4)$$

where $\gamma_{\vec{k}_{\parallel}}=2\cos(k_x)+2\cos(k_y)$. The canting angle $\theta$ is

$$\cos(\theta)=\frac{J_F'}{\sqrt{J_F'^2+J_{\mathrm{AF}}^2}}. \qquad (A5)$$

The parameter $\lambda$ is a Lagrange multiplier, which, at zero temperature, ensures that the spectral weight begins at $\omega=0$, or, alternatively, that $\langle b_{i,j,\uparrow}^{\dagger}b_{i,j,\uparrow}-b_{i,j,\downarrow}^{\dagger}b_{i,j,\downarrow}\rangle=2S$.[37] Equation (A4) was used to obtain the surface spin waves shown in Fig. 6.

---

[1] E. D. Wollan and W. C. Koehler, Phys. Rev. **100**, 545 (1955).

[2] J. M. D. Coey, M. Viret, and S. von Molnar, Adv. Phys. **48**, 167 (1999).

[3] H. Y. Hwang, S.-W. Cheong, N. P. Ong, and B. Batlogg, Phys. Rev. Lett. **77**, 2041 (1996).

[4] Y. Lu, X. W. Li, G. Q. Gong, Gang Xiao, A. Gupta, P. Lecoeur, J. Z. Sun, Y. Y. Wang, and V. P. Dravid, Phys. Rev. B **54**, R8357 (1996).

[5] A. Gupta, G. Q. Gong, G. Xiao, P. R. Duncombe, P. Lecoeur, P. Trouilloud, Y. Y. Wang, V. P. Dravid, and J. Z. Sun, Phys. Rev. B **54**, R15 629 (1996).

[6] N. D. Mathur, G. Burnell, S. P. Isaac, T. J. Jackson, B.-S. Teo, J. L. MacManus-Driscoll, L. F. Cohen, J. E. Evetts, and M. G. Blamire, Nature (London) **387**, 266 (1997).

[7] M. Viret, M. Drouet, J. Nassar, J. P. Coutour, C. Fermon, and A. Fert, Europhys. Lett. **39**, 545 (1997).

[8] J. Z. Sun, D. W. Abraham, K. Roche, and S. S. P. Parkin, Appl. Phys. Lett. **73**, 1008 (1998).

[9] K. Steenbeck, T. Eick, K. Kirsch, H.-G. Schmidt, and E. Steinbeβ, Appl. Phys. Lett. **73**, 2506 (1998).

[10] J. Z. Sun, D. W. Abraham, R. A. Rao, and C. B. Eom, Appl. Phys. Lett. **74**, 3017 (1999).

[11] R. D. Sánchez, J. Rivas, C. Vázquez-Vázquez, A. López-Quntenla, M. T. Causa, M. Tovar, and S. Oseroff, Appl. Phys. Lett. **68**, 134 (1996).

[12] R. Mahesh, R. Mahendrian, A. K. Raychaudhuri, and C. N. R. Rao, Appl. Phys. Lett. **68**, 2291 (1996).

[13] Ll. Balcells, J. Fontcuberta, B. Martínez, and X. Obradors, J. Phys.: Condens. Matter **10**, 1883 (1998).

[14] J. Fontcuberta, B. Martínez, Ll. Balcells, X. Obradors, C. H. Co-henca, and R. F. Jardim, J. Appl. Phys. **83**, 7058 (1998).

[15] Ll. Balcells, J. Fontcuberta, B. Martínez, and X. Obradors, Phys. Rev. B **58**, R14 697 (1998).

[16] H. Y. Hwang and S.-W. Cheong, Nature (London) **389**, 942 (1997).

[17] R. Shreekala, A. Goyal, S. E. Lofland, S. M. Bhagat, K. Ghosh, R. P. Sharma, R. L. Greene, R. Ramesh, and T. Venkatesand, Appl. Phys. Lett. **73**, 2672 (1998).

[18] D. A. Papaconstantopoulos and W. E. Pickett, Phys. Rev. B **57**, 12 751 (1998).

[19] D. Feinberg, P. Germain, M. Grilli, and G. Seibold, Phys. Rev. B **57**, 5583 (1998).

[20] E. Müller-Hartmann and E. Dagotto, Phys. Rev. B **54**, R6819 (1996).

[21] K. H. Ahn and A. J. Millis, Phys. Rev. B **58**, 3697 (1998).

[22] D. I. Khomskii and G. Sawatzky, Solid State Commun. **102**, 87 (1997).

[23] J. van den Brink and D. Khomskii, Phys. Rev. Lett. **82**, 1016 (1999).

[24] A. J. Millis, Phys. Rev. B **55**, 6405 (1997).

[25] T. G. Perring, G. Aeppli, Y. Morimoto, and Y. Tokura, Phys. Rev. Lett. **78**, 3197 (1997).

[26] D. C. Mattis, *The Theory of Magnetism I: Statics and Dynamics* (Springer, New York, 1988).

[27] D. P. Arovas and F. Guinea, Phys. Rev. B **58**, 9150 (1998).

[28] M. J. Calderón and L. Brey, Phys. Rev. B **58**, 3286 (1998).

[29] J.-H. Park, E. Vescovo, H.-J. Kim, C. Kwon, R. Ramesh, and T. Venkatesan, Phys. Rev. Lett. **81**, 1953 (1998).

[30] M. J. Calderón, J. A. Vergés, and L. Brey, Phys. Rev. B **59**, 4170 (1999).

[31] J. A. Vergés, Phys. Rev. B **57**, 870 (1998).

[32] M. Julliere, Phys. Lett. **54A**, 225 (1975).

[33] J. C. Slonczewski, Phys. Rev. B **39**, 6995 (1989).

[34] A. M. Bratkovsky, Phys. Rev. B **56**, 2344 (1997).

[35] F. Guinea, Phys. Rev. B **58**, 9212 (1998).

[36] J. S. Moodera, J. Nowak, and R. J. M. van de Veerdonk, Phys. Rev. Lett. **80**, 2941 (1998).

[37] D. P. Arovas and A. Auerbach, Phys. Rev. B **38**, 316 (1988).